Temperature analysis of a gasket for an internal combustion engine

Dae Kyun Baek and **M M Khonsari***
Department of Mechanical Engineering, Louisiana State University, Baton Rouge, Louisiana, USA

The manuscript was received on 2 March 2005 and was accepted after revision for publication on 24 February 2006.

DOI: 10.1243/09544070JAUTO47

Abstract: This paper presents a heat transfer analysis of a head gasket for an internal combustion (IC) engine. A steady state temperature analysis was conducted to investigate the effect of engine material on gasket temperature. Transient temperature analysis was also conducted to investigate temperature variations of gasket materials and the required time to reach steady state temperature. The transfer of heat from the combustion chamber into the wall (a positive heat flux) which occurs after the ignition and the reverse of this process during the expansion stroke (a negative heat flux) were mathematically represented using the Fourier series.

Keywords: gasket, combustion engine, temperature analysis, heat flux

1 INTRODUCTION

Heat transfer has a pronounced effect on internal combustion (IC) engine performance, efficiency, and emissions [**1–5**]. Complications arise because the heat source in an IC engine requires consideration of chemically reactive flows, and a thorough heat transfer model must take into account the cooling effect that occurs at the cylinder head, the piston, and the gaps between the piston and the cylinder, as well as on the head gasket. It is generally thought that the thermal effect within the head gasket does not significantly affect the overall engine heat transfer characteristics, and therefore it is not taken into consideration. For this reason, there is very little available information in the published literature that could shed light on the thermal performance of gaskets.

A thermal analysis of a gasket is of paramount importance for characterizing the types of gasket failure that are typically encountered in practice [**6**] and for developing techniques that can improve gasket performance. More importantly, unsteady heat effects must be accounted for, particularly if analysis of the root cause of fretting, which is known to cause gasket failure, is of interest. Detailed studies of engine temperature prediction and simulations of combustion chambers are available [**1–5**]. For the purpose of modelling, the gasket is normally considered to be a layer of metal to simplify the thermal analysis [**5**].

The present paper examines the thermal characteristics of a multilayer steel (MLS) gasket. These types of gasket consist of a coating layer bonded to a metallic substrate and beads in the gasket. This paper presents a number of simulations based on numerical solutions of the appropriate equations that govern the heat transfer in the system. All simulations were conducted in two dimensions by Flex-PDE – an FEA software package customized to simulate gasket temperature. The positive and negative surface heat fluxes in the chamber that occur during the engine cycle are modelled using the Fourier series. The time to reach steady state and the temperature variations within the depth of the chamber wall and the gasket were also determined.

2 ANALYSIS

Figure 1 shows a schematic of the combustion chamber to be analysed. In cylindrical coordinates, for an axisymmetric model, the following equation governs the transient, two-dimensional

* *Corresponding author: Department of Mechanical Engineering, Louisiana State University, 2508 CEBA, Baton Rouge, Louisiana, 70803, USA. email: khonsari@me.lsu.edu*

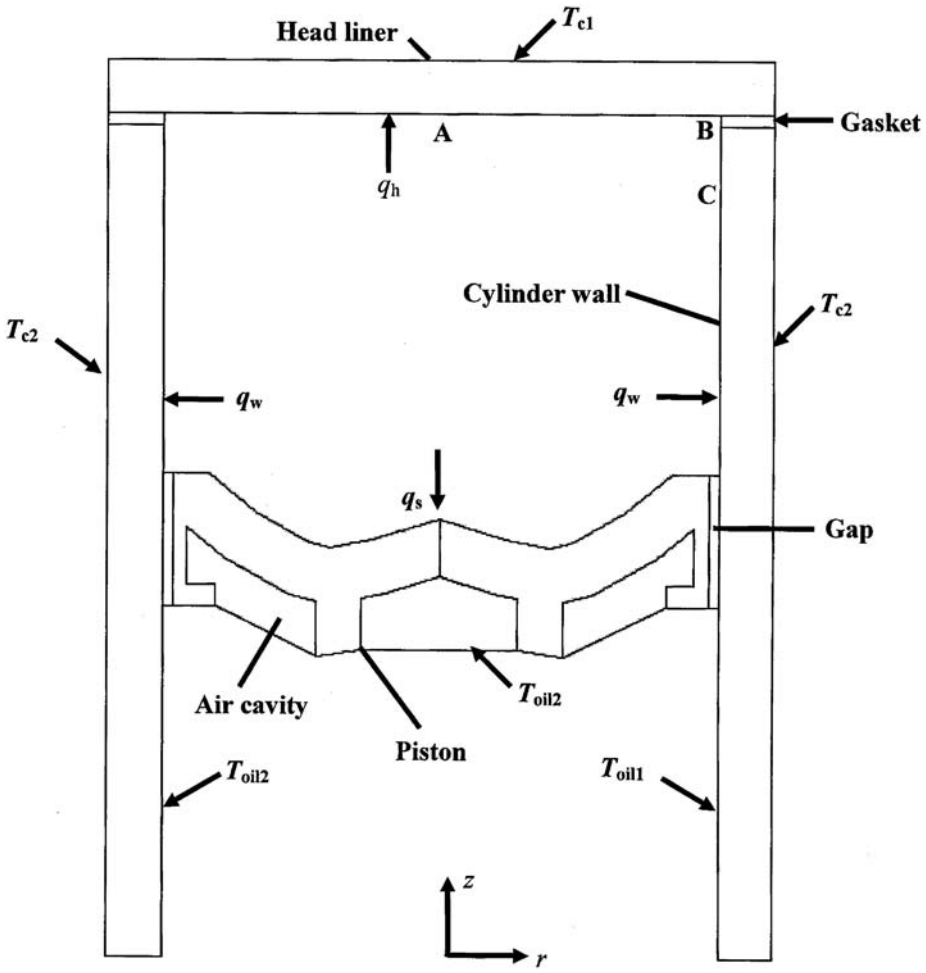

Fig. 1 Model of a whole combustion chamber

heat conduction

$$\frac{1}{r}\frac{\partial}{\partial r}\left(kr\frac{\partial T}{\partial r}\right)+\frac{\partial}{\partial z}\left(k\frac{\partial T}{\partial z}\right)=\rho c_p\frac{\partial T}{\partial t} \quad (1)$$

where r and z are the coordinates in the radial and axial directions respectively, T is temperature, k is the thermal conductivity, ρ is the material density, c_p is the specific heat, and t is time.

To analyse the gasket temperature, a model of a full combustion chamber and a model of a partial combustion chamber were developed. A steady state thermal analysis was performed to compare both models, and transient thermal analysis was carried out using the model of a partial combustion chamber. The right-hand side of equation (1) is equal to zero in the case of steady state heat conduction.

The boundary conditions imposed are as follows [**5**]. The temperatures on the outer surface of the cylinder wall, head, and piston are treated as constant surface temperature conditions, i.e. the so-called Dirichlet condition is imposed there. The magnitude of the temperature is equal to either the measured coolant temperature or the oil temperature in the crankshaft case. The appropriate parameters are the temperature of the cylinder head, T_{c1}, the coolant temperature, T_{c2}, the temperature on the bottom surface of the piston, T_{oil1}, and the temperature on the inner surface of the cylinder wall below the piston, T_{oil2}.

An MLS gasket is located between the cylinder wall and the head. The air thermal conductivity is used to model the appropriate regions between cylinder wall and piston. The conductivity of carbon steel is used to represent the piston rings. In order to determine the gasket temperature distributions, a simplified model of a partial chamber (Fig. 2) was developed. The gasket is modelled as a single-layer body with the same thickness as an MLS with a rubber coating on both sides. The gasket has the rubber coating to prevent the cylinder from leakage. The diameter of the cylinder bore is 78 mm, the

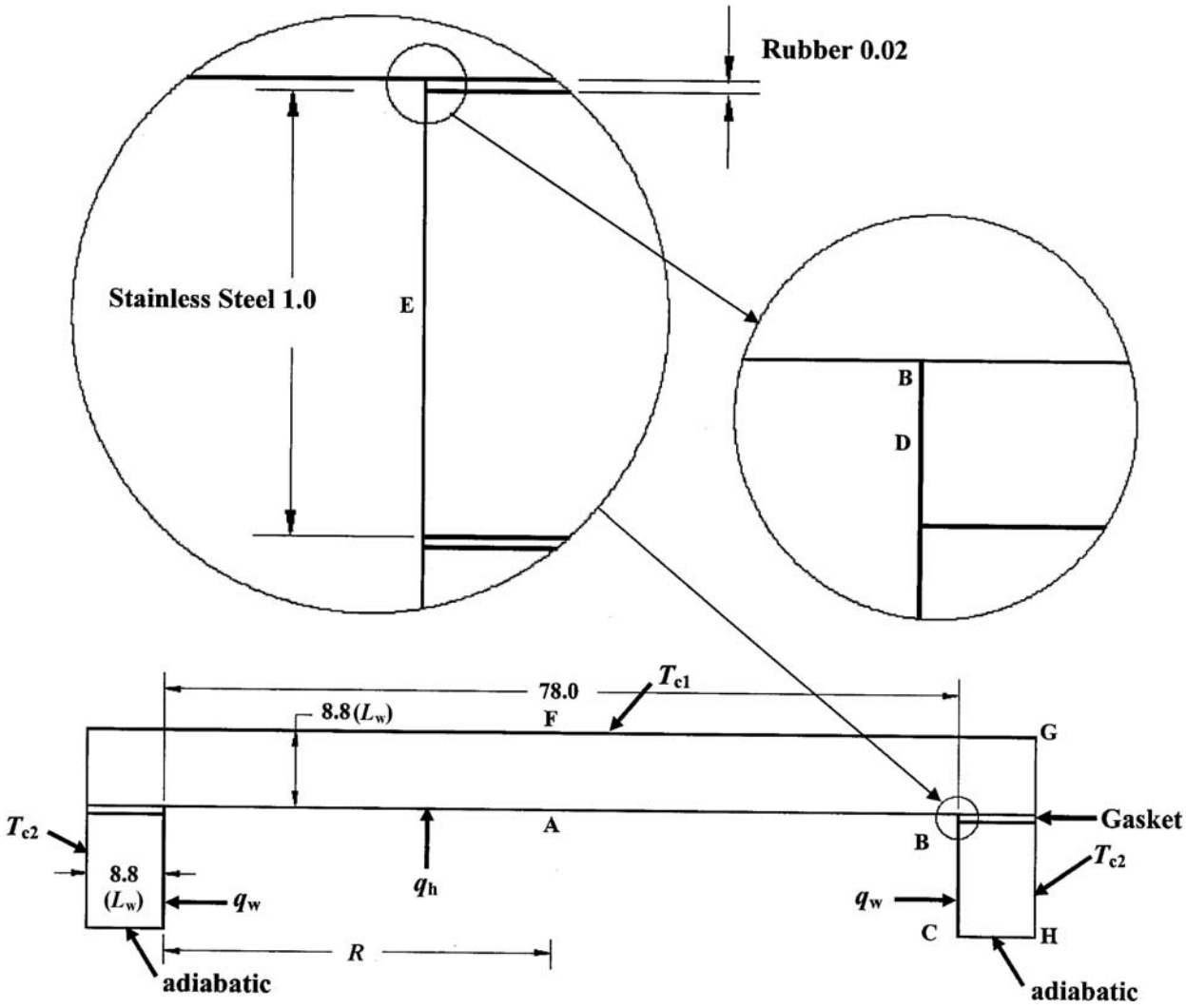

Fig. 2 Model of a partial combustion chamber

thicknesses of the cylinder wall and the cylinder head are both 8.8 mm, the thickness of the rubber coating is 0.02 mm, and the thickness of the stainless steel is 1 mm. Also shown in Fig. 2 is the area where the adiabatic boundary condition applies in the partial chamber model.

Nijeweme *et al.* [**7**] reported that positive heat flux from the combustion chamber into the wall mostly occurs around the top dead centre (TDC) after ignition, and negative heat flux from the wall into the combustion chamber occurs during the expansion stroke, even though the bulk gas temperature is higher than the wall temperature. The surface heat flux depends on the location of the chamber, the ignition timing, the engine speed, the combustion temperature, and the cylinder pressure [**7–9**].

Following the work of Nijeweme, the surface heat flux is modelled using the Fourier series. The implementation of both the heat flux and the time delay between the positive and the negative heat flux requires some discussion. Figure 3 is an illustration of the surface heat flux in the inside partial chamber. The functions $q_p(t)$ and $q_n(t)$ are the time-dependent positive and negative heat fluxes in the chamber respectively. In Fig. 3, the cycle time is t_c, the time duration of the positive heat flux is t_p, the time duration of the negative heat flux is t_n, and the time difference between the positive and the negative heat fluxes is t_d. The time-dependent positive heat flux function $q_p(t)$ is

$$q_p(t) = q_{ap} u_1(t) \tag{2}$$

where q_{ap} is the amplitude of the positive heat flux and $u_1(t)$ is the Fourier series of a square wave of the form for the positive heat flux

$$u_1(t) = a_0 + \sum_{m=1}^{\infty} (a_m \cos m\pi t + b_m \sin m\pi t) \tag{3}$$

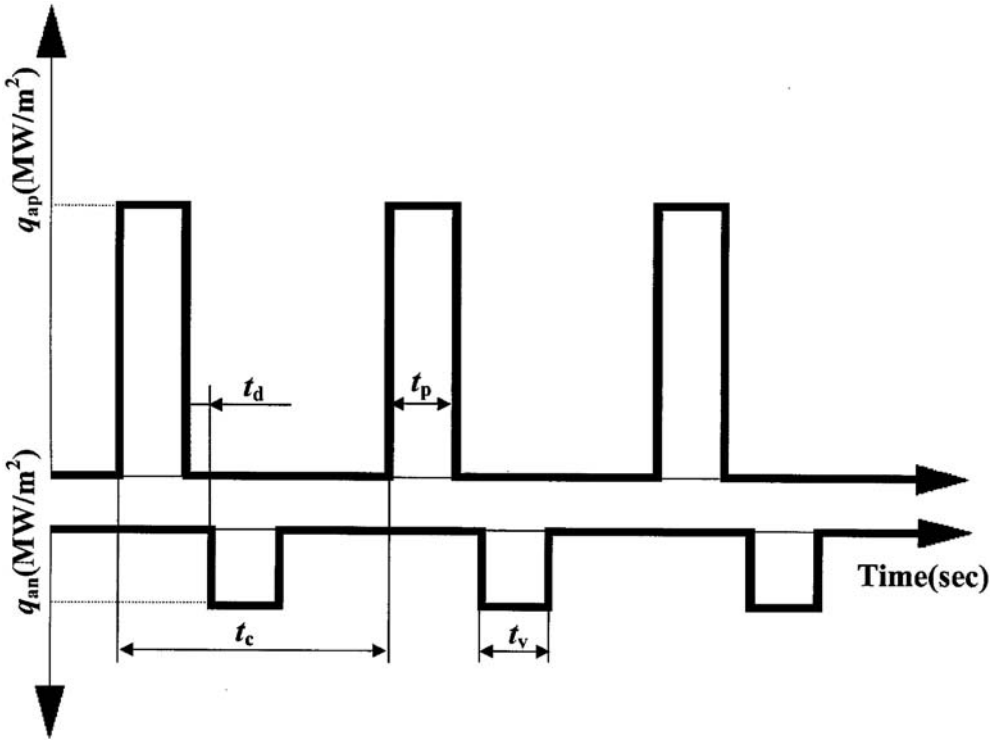

Fig. 3 Schematic model of the surface heat flux in the combustion chamber

The time-dependent negative heat flux function $q_n(t)$ is as follows

$$q_n(t) = -q_{an}u_2(t) \tag{4}$$

where q_{an} is the amplitude of the negative heat flux and $u_2(t)$ is the Fourier series of a square wave of the form for the negative heat flux

$$u_2(t) = c_0 + \sum_{m=1}^{\infty} (c_m \cos m\pi t + d_m \sin m\pi t) \tag{5}$$

For the steady state and transient temperature analyses in two dimensions, a commercially available FEA software package, Flex-PDE, was used. The mesh (element) sizes in the rubber coating and in the gasket were approximately 4 and 10 μm respectively.

2.1 Non-dimensional analysis

In this section, non-dimensional parameters are introduced so that the results can be used more universally. The dimensionless temperature and spatial coordinates are as follows

$$\theta^* \equiv \frac{\theta}{\theta_{max}} = \frac{T - T_{c1}}{T_{max} - T_{c1}} \tag{6}$$

$$r^* \equiv \frac{r}{R} \tag{7}$$

$$z^* \equiv \frac{z}{L} \tag{8}$$

where R and L are the radius and height of the cylinder bore respectively. The Fourier number, Fo, is defined as

$$Fo = \frac{\alpha t}{R^2} \tag{9}$$

where $\alpha = k/(\rho c_p)$. A dimensionless time may be defined as

$$t^* \equiv \frac{\alpha t}{R^2} \equiv Fo \tag{10}$$

where t^* is equivalent to the dimensionless Fourier number. Substituting equations (6) to (10) into equation (1) yields the heat equation

$$\frac{1}{r^*}\frac{\partial}{\partial r^*}\left(r^*\frac{\partial \theta^*}{\partial r^*}\right) + \Lambda_1^2\frac{\partial^2\theta}{\partial z^{*2}} = \frac{\partial \theta^*}{\partial Fo} \tag{11}$$

where $\Lambda_1 = R/L$. The Biot numbers, Bi_r and Bi_z, are defined as

$$Bi_r = \frac{hR}{k} \tag{12}$$

$$Bi_z = \frac{hL}{k} \tag{13}$$

2.1.1 Heat flux

The dimensionless positive heat flux is

$$q_{\mathrm{p}}^{*} = \frac{q_{\mathrm{p}}}{q_{\mathrm{ap}}} = u_1(t^{*}) \tag{14}$$

where

$$u_1(t^{*}) = a_0 + \sum_{m=1}^{\infty} (a_m \cos \beta_1 m\pi t^{*} + b_m \sin \beta_1 m\pi t^{*}),$$
$$\beta_1 = \frac{R^2}{\alpha} \tag{15}$$

and the dimensionless negative heat flux is

$$q_{\mathrm{n}}^{*} = \frac{q_{\mathrm{n}}}{q_{\mathrm{ap}}} = -\frac{q_{\mathrm{np}}}{q_{\mathrm{ap}}} u_2(t^{*}) \tag{16}$$

where

$$u_2(t^{*}) = c_0 + \sum_{m=1}^{\infty} (c_m \cos \beta_1 m\pi t^{*} + d_m \sin \beta_1 m\pi t^{*}) \tag{17}$$

Independent parameters governing the heat flux are t_{c}^{*}, t_{d}^{*}, t_{v}^{*}, and t_{p}^{*}.

2.1.2 Initial and boundary conditions for the partial combustion chamber

When the initial temperature is equal to T_{c1}, $T_{\mathrm{c1}} = T_{\mathrm{c2}}$ and the outer chamber has a convection boundary condition. The initial and boundary conditions with the thickness of the cylinder wall, L_{w}, become

$$\theta^{*}(r^{*}, 0) = 0 \tag{18}$$

$$\theta^{*}(z^{*}, 0) = 0 \tag{19}$$

$$\left.\frac{\partial \theta^{*}}{\partial r^{*}}\right|_{r^{*}=1} = -\beta_2 (q_{\mathrm{p}}^{*} + q_{\mathrm{n}}^{*}) \tag{20}$$

$$\left.\frac{\partial \theta^{*}}{\partial z^{*}}\right|_{z^{*}=1} = -\beta_3 (q_{\mathrm{p}}^{*} + q_{\mathrm{n}}^{*}) \tag{21}$$

where

$$\beta_2 = \frac{R}{T_{\max} - T_{\mathrm{c1}}}, \qquad \beta_3 = \frac{L}{T_{\max} - T_{\mathrm{c1}}}$$

and

$$\left.\frac{\partial \theta^{*}}{\partial r^{*}}\right|_{r^{*}=1+\Lambda_2} = -Bi_r \theta^{*}(1 + \Lambda_2, t^{*}) \tag{22}$$

$$\left.\frac{\partial \theta^{*}}{\partial r^{*}}\right|_{z^{*}=1+\Lambda_3} = -Bi_z \theta^{*}(1 + \Lambda_3, t^{*}) \tag{23}$$

where

$$\Lambda_2 = \frac{L_{\mathrm{w}}}{R}, \qquad \Lambda_3 = \frac{L_{\mathrm{w}}}{L}$$

3 RESULTS AND DISCUSSION

3.1 Steady state temperature analysis of the gasket

Schematics of a full chamber and a partial chamber are shown in Figs 1 and 2 respectively. The chamber, the piston, the air cavity, the piston ring, the coolant, and the oil temperatures were considered in the full chamber. The part of the chamber around the gasket and the cylinder head is taken into account in the partial chamber model.

3.1.1 Cast iron cylinder head and cast iron cylinder wall

The material of the cylinder, the head, and the piston ring was cast iron, and the piston was aluminium. The gasket consisted of stainless steel (SS) and the rubber coating. The heat fluxes q_{h}, q_{w}, and q_{p} were specified to be 0.8 MW/m^2. The material properties evaluated at room temperature are shown in Table 1. These properties are assumed to remain constant. The temperatures above the cylinder head and outside the cylinder wall were specified to remain at the coolant temperature, i.e. $T_{\mathrm{c1}} = T_{\mathrm{c2}} = 80\,^{\circ}\mathrm{C}$. Temperatures T_{oil1} and T_{oil2} were 150 and 100 °C respectively, i.e. the same as the oil temperature.

Figure 4(a) shows a comparison between the chamber surface temperature of the full model and that of the partial model. In this figure, the d coordinate represents the location along the chamber surface from point A to C through B, as shown in Figs 1 and 2. The results show that the surface temperature of the partial model is almost the same as that of the full chamber. This implies that the temperature distribution of the gasket is not appreciably affected by the presence of the piston. There is a temperature difference between the full chamber

Table 1 Material properties for gasket temperature analysis at room temperature (20 °C)

	k (W/m K)	ρ (kg/m^3)	c_p (J/kg K)
Aluminium	185	2700	900
Cast iron	47.65	7890	447
Stainless steel	16.2	8000	500
Rubber	0.5	1180	1600
Air	0.04	0.7	1029.5

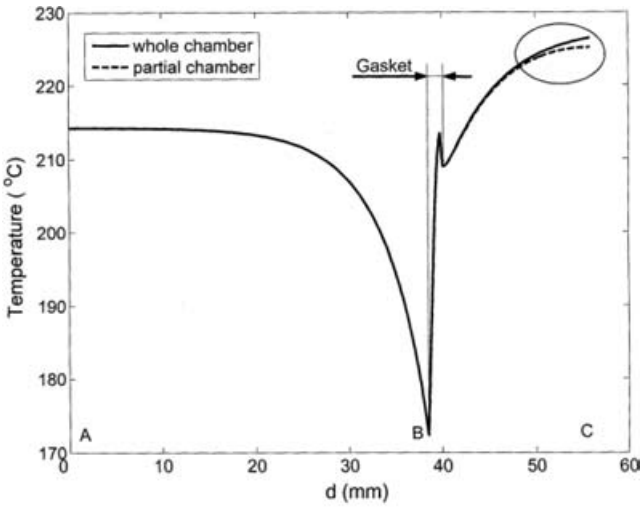

(a) comparison between the whole and the partial combustion chamber

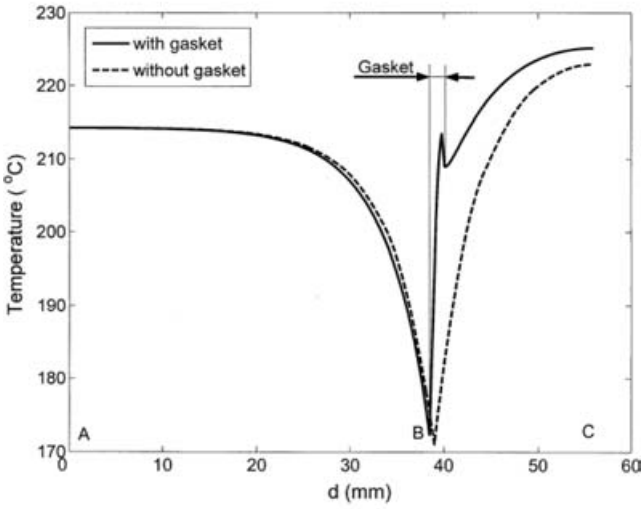

(b) surface temperature with and without gasket

Fig. 4 Surface temperature of the cast iron cylinder head and the cast iron cylinder wall ($T_{c1} = T_{c2} = 80\ ^\circ$C)

model and the partial model in the vicinity of the adiabatic boundary condition, as shown in the inset in Fig. 4(a). The distance from the gasket to the boundary where the partial model was separated from the whole chamber was about 20 mm. This is found to be adequate for analysing the gasket temperature. The temperature distribution of the gasket is mostly affected by the cylinder head and the wall near the gasket because most of the heat in the chamber transfers radially to the cylinder wall and axially towards the cylinder head. As shown in Fig. 4(a), a temperature gradient exists in the gasket owing to the thermal conductivity difference between the cylinder head, the cylinder wall, and the gasket. The temperature in region C is highest, followed by the temperature in region A, and the temperature in region B is lowest. The surface temperature of the chamber without a gasket is shown in Fig. 4(b) for comparison. It can be seen that the presence of the gasket tends to increase the temperature of the cylinder wall because the thermal conductivity of stainless steel and rubber is less than that of cast iron.

The cylinder head, the cylinder wall, the coolant temperature, and the heat flux are important as far as the temperature of the gasket is concerned. To determine the effect of the cylinder head, a set of simulations was performed where the temperature above the cylinder head was specified as $T_{c1} = 150\ ^\circ$C. All boundary conditions and the heat flux are the same as in Fig. 4(b), except $T_{c1} = 150\ ^\circ$C. The result of prediction for the surface temperature along ABC is shown in Fig. 5(a). The results show that the maximum temperature occurs in region A. As shown in Fig. 5(a), the gasket temperature with $T_{c1} = 150\ ^\circ$C is much higher than that with $T_{c1} = 80\ ^\circ$C. The high temperature gradients between the cylinder and the gasket and between the cylinder wall and the gasket could contribute to high thermal stresses.

3.1.2 *Aluminium cylinder head and cast iron cylinder wall*

Aluminium is being used as a cylinder head material in many combustion engines. This section compares the performance of an aliminium cylinder head and a cast iron cylinder wall. The result of simulations is shown in Fig. 5(b). The boundary conditions and the heat flux are the same as those shown in Fig. 4, with $q_h = q_w = 0.8$ MW/m^2 and $T_{c1} = T_{c2} = 80\ ^\circ$C. The surface temperature with $T_{c1} = 150\ ^\circ$C is also shown in Fig. 5(b). Because of a large difference in the thermal conductivity, the temperature difference becomes significant at different interfaces between the cylinder head and the gasket, resulting in undesirable thermal stress at those locations.

3.1.3 *Aluminium cylinder head and aluminium cylinder wall*

Figure 5(c) shows the results of simulations assuming that both the cylinder head and cylinder wall are made of aluminium. The boundary conditions and the heat flux are the same as in Fig. 4, with $q_h = q_w = 0.8$ MW/m^2 and $T_{c1} = T_{c2} = 80\ ^\circ$C. The surface temperature with $T_{c1} = 150\ ^\circ$C is also shown in Fig. 5(c) for comparison. The maximum temperature occurs at the gasket surface because both the cylinder head and the cylinder wall have high thermal conductivity.

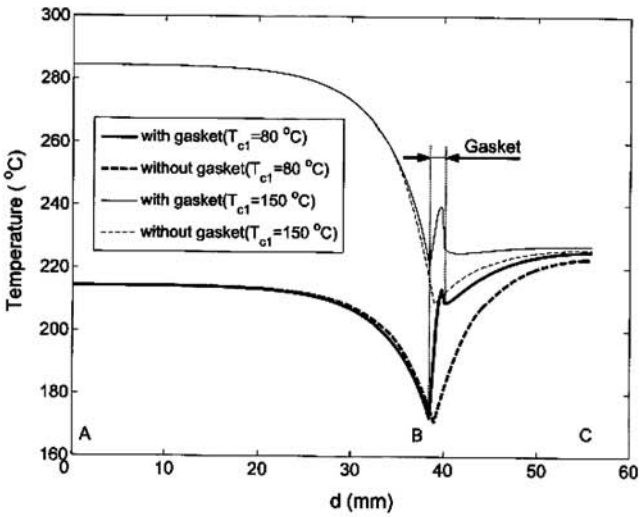

(a) cast iron cylinder head and cast iron cylinder

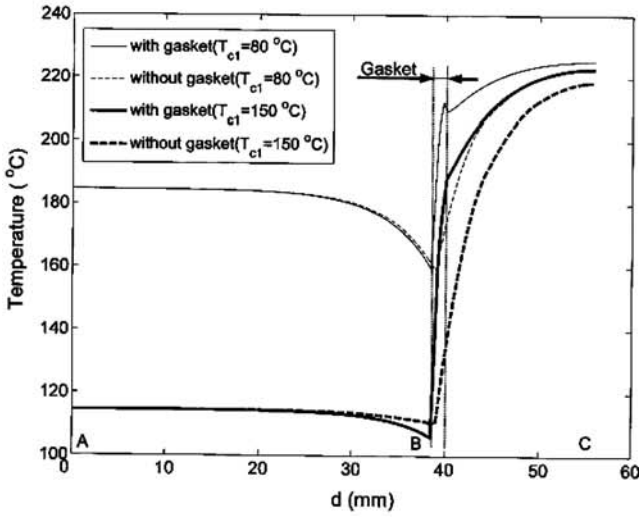

(b) aluminium cylinder head and cast iron cylinder

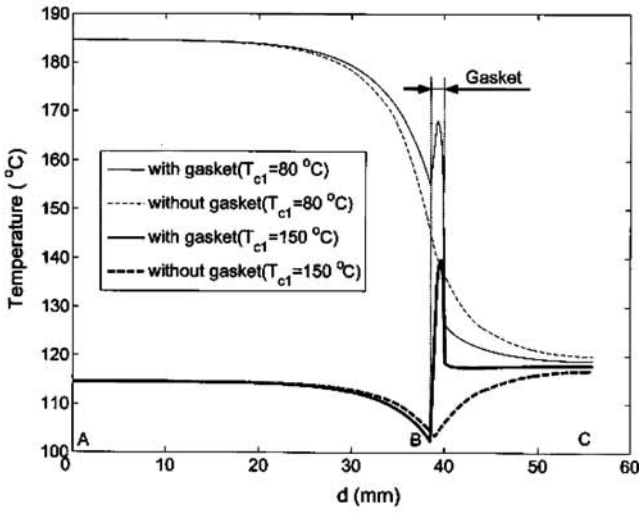

(c) aluminium cylinder head and aluminium cylinder

Fig. 5 Combustion wall surface temperature with varying engine materials with and without a gasket

Large temperature differences occur not only between the gasket and the cylinder head but also between the gasket and the cylinder wall.

3.2 Transient temperature analysis of the gasket

3.2.1 Constant temperature boundary conditions

This section gives the results of transient temperature simulations in both cast iron head and wall using the partial chamber model. Only the positive surface heat flux on the inside of the chamber was used in the case of constant temperatures on the outer surface of the chamber. As mentioned earlier, the surface heat flux depends on many variables. In this paper, the heat flux value as specified in reference [**7**] is used, assuming it remains constant over the chamber. For this purpose, $q_{ap} = 3.2\ \mathrm{MW/m^2}$ lasting for one stroke is assumed. This value is four times the steady state heat flux. The total length of the time for four strokes is assumed to be 0.06 s (corresponding to about 2000 r/min). The positive heat fluxes q_h and q_w in Fig. 2 are specified as given in equation (2).

The selected number of terms in the Fourier series for heat flux was 10, considering the extensive computational time that is required for the execution of the computer program. The temperature above the cylinder head and outside the cylinder wall was specified to be $T_{c1} = T_{c2} = 80\ ^\circ\mathrm{C}$, i.e. the same as the coolant temperature.

The transient temperatures of the cylinder head at A, the gasket at E, and the rubber at D are shown in Fig. 6. The quasi steady state temperatures at A, E, and D in Fig. 6 are similar to those in Fig. 4. The amplitudes of temperature fluctuation induced by the transmitted heat flux are large, particularly in the rubber coating as shown in Fig. 6(c). This implies that the fluctuating temperature could cause high thermal stress on the gasket materials.

The time required to reach steady state is about 6 s – a relatively short time – because it was assumed that the coolant temperature and the initial temperature of the engine were both at 80 °C. This may occur when the engine starts again after stopping the engine briefly.

3.2.2 Convection boundary conditions

In order to determine the time required to reach the quasi steady state from the engine start-up, a heat convection coefficient had to be assumed for the outer surfaces of both the cylinder head and the cylinder wall. Both positive and negative heat fluxes

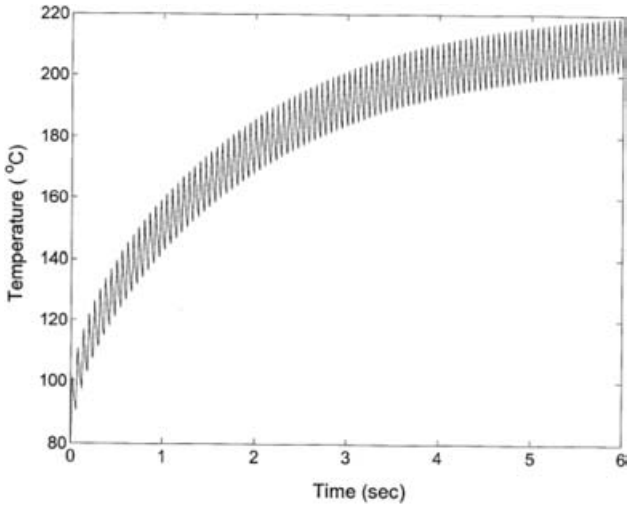

(a) cylinder head at 'A'

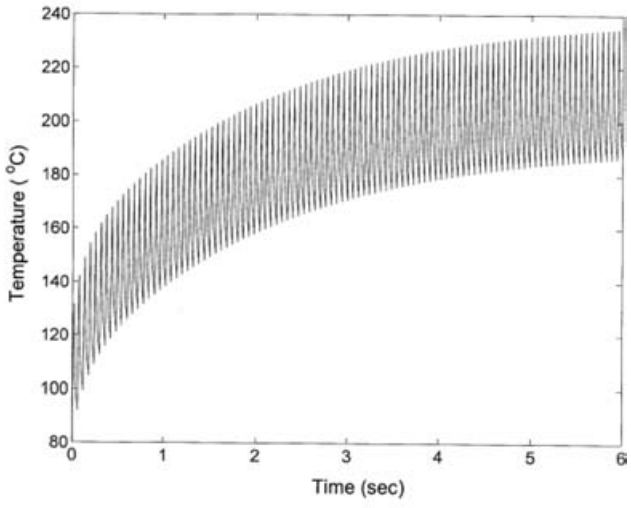

(b) gasket at 'E'

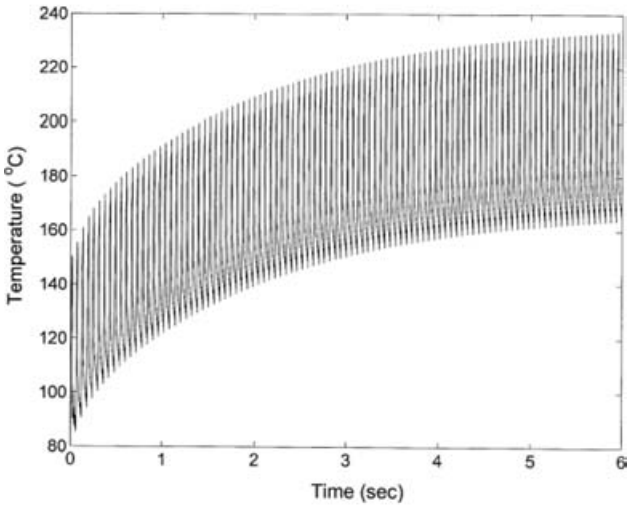

(c) rubber at 'D'

Fig. 6 Transient surface temperature of the combustion wall with constant temperature boundary conditions

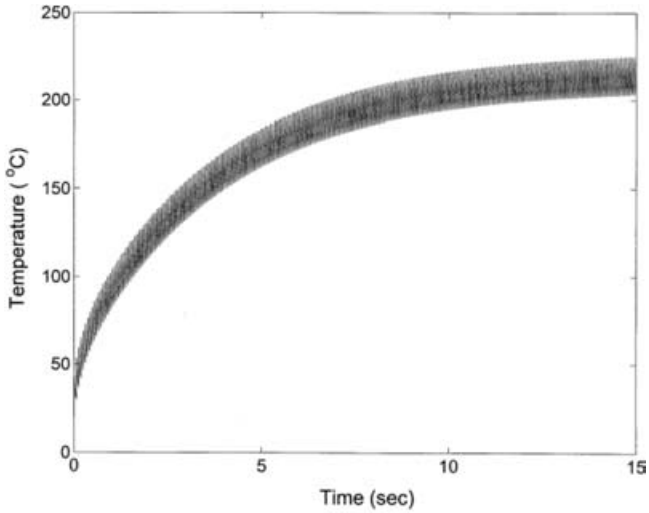

(a) cylinder head at 'A'

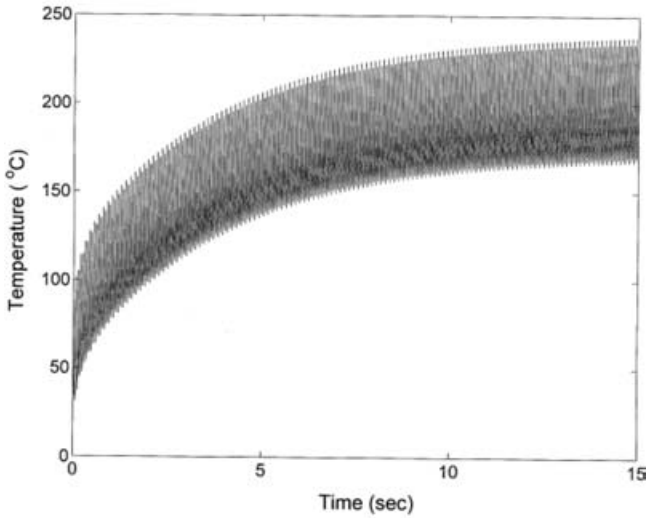

(b) gasket at 'E'

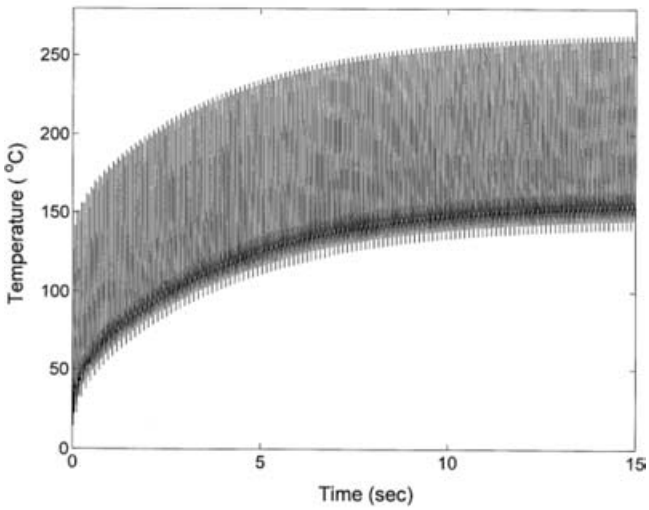

(c) rubber at 'D'

Fig. 7 Transient surface temperature of the combustion wall with convection boundary conditions

were used in the case of a convection boundary condition on the outer surface of the chamber. In Fig. 3, the cycle time is $t_c = 0.06$ s, the time duration of the positive heat flux $t_p = 0.008$ s, the time duration of the negative heat flux $t_n = 0.015$ s (one stroke), and the time difference between the positive and negative heat fluxes $t_d = 0.002$ s. It was assumed that the amplitude of positive heat flux $q_{ap} = 6.4$ MW/m^2 and the amplitude of negative heat flux $q_{an} = 0.4$ MW/m^2. The total heat flux for four strokes is 0.8 MW/m^2, i.e. the same as steady state analysis.

Heat transfer from the walls of the cylinder head to the coolant is assumed to take place by a combination of forced convection and subcooled, nucleate boiling [**10**]. It is widely known that the forced convection coefficient of water is about 300–10 000 W/(m^2 K) [**11**]. However, to determine the coolant heat flux accurately, the properties and the velocity of the liquid coolant must be known [**12**]. In this research it was assumed that the heat transfer of coolant takes place by convection. The initial temperature of the engine and the coolant temperature were considered to be 20 °C. The heat convection coefficient for the coolant was specified to be 2000 W/(m^2 K). This was chosen by a trial and error method, making the surface temperatures of both the cylinder head and the cylinder wall the same as those of the steady state analysis in Fig. 4.

The transient temperatures of the cylinder head at A, the gasket at E, and the rubber at D are shown in Fig. 7. The time required to reach the quasi steady state from the engine start is about 15 s.

The surface temperature of the outer chamber along FGH after the quasi steady state is shown in Fig. 8. The temperature at the outer corner between the cylinder head and the cylinder wall is much less than the constant surface temperature condition maintained at 80 °C because Fig. 8 describes the temperature distributions at the beginning of the engine start-up period whereas Fig. 6 describes them after the coolant has been heated up.

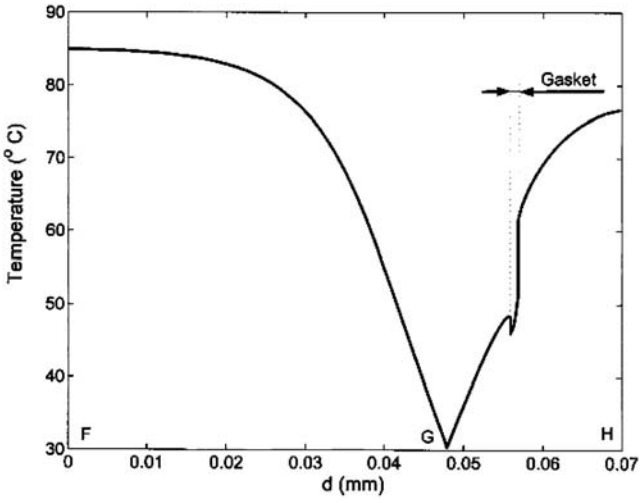

Fig. 8 Surface temperature of the outer chamber along FGH

Figure 9(a) displays the transient temperature variation at different depths into the cylinder head below the head surface temperature. Figures 9(b) and (c) are for the gasket and for the rubber respectively. It can be concluded in all the cases simulated that the transient temperature variation is confined to a depth of about 1 mm. Below this depth, the influence of transient temperature variation becomes nil. The amplitude of the temperature variation in the rubber coating is very large. This variation is confined to a small depth within the rubber coating and becomes negligibly small at greater depths.

4 CONCLUSIONS

A steady state and transient study of a head gasket temperature is presented. The results are restricted to two-dimensional simulations. It is shown that the partial chamber model is valid for gasket temperature analysis because most of the heat in the chamber transfers radially to the cylinder wall and the heat transferred to the cylinder wall in the axial direction is negligibly small. Results show that there exist high temperature gradients, about 30–60 K, in the gasket owing to the thermal conductivity difference between the gasket and the engine. When the engine material is made of aluminium, the gradient is very high. The rubber coating used in gaskets is partly responsible for this high temperature gradient, because of its low thermal conductivity. This temperature difference, along with the difference in thermal expansion coefficients between the engine and the gasket, could cause high thermal stress.

The positive and negative heat fluxes in the inside cylinder were modelled using the Fourier series, and the transient temperature of the gasket was also simulated. Low thermal conductivity causes high surface temperature fluctuation under an imposed heat flux. Thus, the temperature of the rubber undergoes a considerable amount of fluctuation.

When a constant coolant temperature was used as a boundary condition, the time required to reach the quasi steady state was only 6 s. The simulations predict that the time required to reach the quasi steady state from engine start-up was about 15 s.

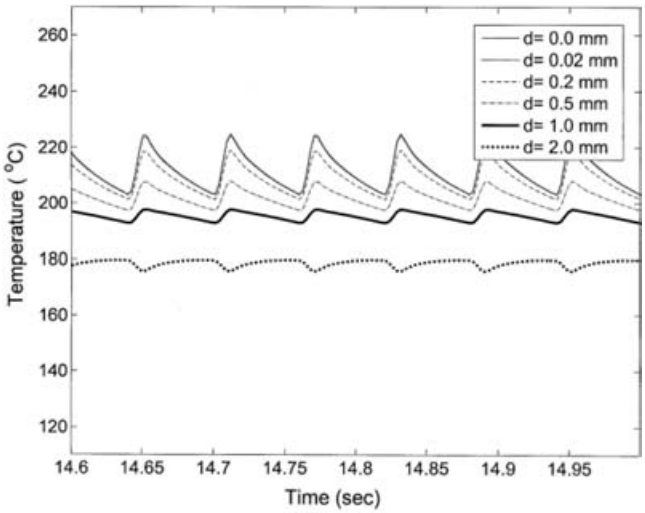

(a) cylinder head at 'A'

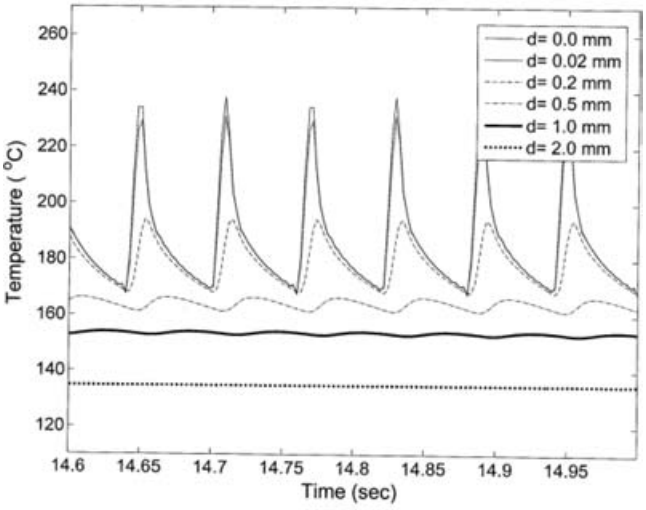

(b) gasket at 'E'

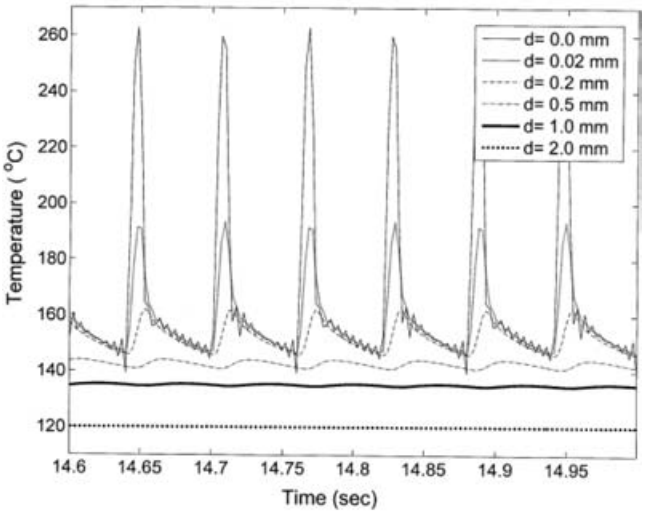

(c) rubber at 'D'

Fig. 9 Temperature variation with depth into the combustion wall

Therefore, understanding the transient temperature analysis is also very important in predicting the behaviour of IC engines.

REFERENCES

1 **Borman, G. L.** and **Nishiwaki, K.** Internal combustion engine heat transfer. *Progress in Energy Combust. Sci.*, 1987, **13**, 1–46.
2 **Han, Z.** and **Reitz, R. D.** Temperature wall function formulation for variable-density turbulent flow with application to engine convective heat transfer modeling. *Int. J. Heat and Mass Transfer*, 1997, **40**(3), 613–625.
3 **Liu, Y.** and **Reitz, R. D.** Multidimensional modeling of engine combustion chamber surface temperatures. SAE paper 971593, 1997.
4 **Sunayama, N.** Heat transfer/thermal analysis for cylinder head. SAE paper 910301, 1991.
5 **Liu, Y.** and **Reitz, R. D.** Modeling of heat conduction within chamber walls for multidimensional internal combustion engine simulations. *Int. J. Heat and Mass Transfer*, 1998, **41**, 859–969.
6 **Kestly, M., Popielas, F., Grafl, D.,** and **Weiss, A.** Accelerated testing of multi-layer steel cylinder head gaskets. SAE paper 011188, 2000.
7 **Nijeweme, D., Kok, J., Stone, C.,** and **Wyszynski, L.** Unsteady in-cylinder heat transfer in a spark ignition engine: experiments and modeling. *Proc. IMechE, Part D: J. Automobile Engineering*, 2001, **215**, 747–760.
8 **Alkidas, A. C.** Heat transfer characteristics of a spark-ignition engine. *Trans. ASME, J. Heat Transfer*, 1980, **102**, 189–193.
9 **Gatowski, J. A., Smith, M. K.,** and **Alkidas, A. C.** Experimental investigation of surface thermometry and heat flux. *Expl Thermal and Fluid Sci.*, 1989, **2**, 280–292.
10 **Collier, J. G.** and **Thome, J. R.** *Convective Boiling and Condensation*, 1972, pp. 211–214 (McGraw-Hill, London).
11 **Sparrow, E. M.** and **Gregg, J. L.** Laminar free convection from a vertical flat plate with uniform surface heat flux. *Trans. ASME*, 1956, **78**, 435–440.
12 **Finlay, I. C., Harris, D., Boam, D. J.,** and **Parks, B. I.** Factors influencing combustion chamber wall temperatures in a liquid-cooled, automotive, spark-ignition engine. *Proc. IMechE, Part D: J. Automobile Engineering*, 1985, **199**, 207–214.

APPENDIX

Notation

a	amplitude of oscillatory motion
a_0, a_m, b_m	constants in evaluating the Fourier series function of $u_1(t)$

c_0, c_m, d_m	constants in evaluating the Fourier series function of $u_2(t)$
c_p	specific heat
f	frequency of oscillatory motion
k	thermal conductivity
L	height of the partial cylinder bore
L_w	thickness of the cylinder wall
q_{an}	amplitude of the negative heat flux
q_{ap}	amplitude of the positive heat flux
q_h	heat flux towards the cylinder head
$q_n(t)$	time-dependent negative heat flux towards the chamber
$q_p(t)$	time-dependent positive heat flux towards the cylinder wall
q_s	heat flux towards the piston
q_w	heat flux towards the cylinder wall
r	radial coordinate
R	radius of the cylinder bore
T	temperature
T_a	temperature of the air
T_{c1}	temperature of the cylinder head
T_{c2}	coolant temperature
T_{max}	maximum possible temperature
T_{oil1}	temperature on the bottom surface of the piston
T_{oil2}	temperature on the inner surface of the cylinder wall below the piston
t	time
t_c	cycle time of the engine
t_d	time difference between the positive and the negative heat flux
t_n	time duration of the negative heat flux
t_p	time duration of the positive heat flux
$u_1(t)$	Fourier series of a square wave of the form for positive heat flux
$u_2(t)$	Fourier series of a square wave of the form for negative heat flux
z	axial coordinate
θ^*	dimensionless temperature
ρ	material density